

Tunable multi-magnon Floquet topological edge states

I. Martinez-Berumen,^{1,*} T. Pereg-Barnea,^{1,†} and W. A. Coish^{1,‡}

¹*Department of Physics, McGill University, Montréal, Québec, Canada H3A 2T8*

(Dated: February 6, 2026)

We show that periodically time-modulating the Dzyaloshinskii-Moriya interaction (DMI) in a two-dimensional magnon insulator may induce a topological phase transition that results in the presence of robust edge modes. To this end, we study a square lattice of spins interacting via an XXZ Heisenberg model with a ferromagnetic longitudinal coupling and antiferromagnetic transverse coupling, as well as the aforementioned time-modulated DMI. The topologically protected edge states of this system are composed of coherent superpositions of single-magnon excitations and two-magnon bound states. Furthermore, we show that the chirality of the edge states can be controlled by adjusting the relative phase for the drive on the DMI associated with nearest neighbors in the x and y directions.

I. INTRODUCTION

The study of topological band structures has been extended from electronic systems [1–3] to other areas such as photonics [4, 5], cold atoms [6, 7], and quantum magnetism [8–13]. The topological magnon insulator (TMI) was proposed in 2013 by Zhang *et al.* [9] motivated by the prediction of the magnon thermal Hall effect [14–16] and its experimental observation in $\text{Lu}_2\text{V}_2\text{O}_7$ [17, 18]. TMIs are the magnonic analogues of Chern insulators, which host the quantum Hall effect [19–21]. Their band structure is often studied using linear spin-wave theory, where the Holstein-Primakoff transformation [22] is applied to the spin Hamiltonian to obtain a bosonic system whose excitations (magnons) consist of a coherent superposition of single local spin-flip excitations out of the ferromagnetic ground state. In linear spin-wave theory, magnon-magnon interactions are neglected (in the low-temperature/dilute limit) and the Chern numbers of the free-magnon bands are used to distinguish between topologically trivial and topologically nontrivial phases. The bulk-boundary correspondence predicts the existence of robust propagating edge states when the magnon insulator is in the nontrivial phase [23]. This robustness makes TMIs interesting for potential applications in spin-wave devices like spin-wave diodes, splitters, and interferometers [24, 25], and in potentially generating a strong coherent coupling between distant spins for quantum computing [26].

Magnon-magnon interactions come into play when at least two spin-flip excitations become probable. These interactions may alter the properties of a magnetic system, for example, by stabilizing a topological phase [27] or destroying it [28]. For sufficiently strong attractive interactions, which are present in anisotropic quantum magnets, two local spin flips may bind together, forming a two-magnon bound state (TMBS) with lower energy than two

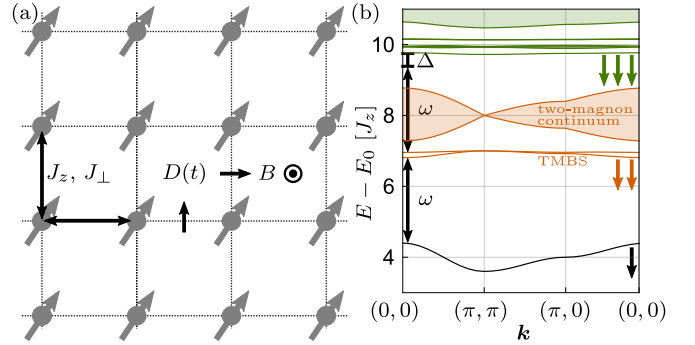


FIG. 1. (a) Square lattice of spins with nearest-neighbor anisotropic spin-spin couplings (J_z , J_\perp), a time-modulated Dzyaloshinsky-Moriya interaction (DMI), $D(t)$, and a longitudinal Zeeman field B . (b) Energies for the single-magnon states (black \downarrow), two-magnon states (orange, above $\downarrow\downarrow$), and three-magnon states (green, above $\downarrow\downarrow\downarrow$) that are energies of the static Hamiltonian H_S [Eq. (2)]. The DMI is modulated with frequency ω so that it resonantly couples the single-magnon band to the two-magnon bound state (TMBS), but the modulation frequency is detuned by Δ from resonance with the three-magnon states. The spectrum is obtained by exact diagonalization (see Appendix A) in a 7×7 lattice. The energy $E - E_0$ for each state is shown here relative to the ground state energy E_0 [Eq. (7)] using $J_\perp = J_z/5$, $B = 2J_z$.

separated spin flips [29–31]. The two-magnon spectrum is then divided into two components: The lower-energy part of the spectrum contains discrete TMBSs and the higher-energy part of the spectrum shows a two-magnon continuum, which may approximately describe two independent magnons [see Fig. 1(b)]. TMBSs have been observed experimentally in both ferromagnetic and antiferromagnetic systems [32–34] and their dynamics have been simulated using cold atoms in optical lattices [35]. Furthermore, it has been proposed that the TMBS spectrum can be topologically nontrivial, resulting in robust edge states comprising a coherent superposition of local two-spin-flip pairs [36, 37].

In systems where the total number of magnons is not conserved, it may be that magnonic excitations consist of hybridized single-magnon and two-magnon states [38–

* pablo.martinez2@mail.mcgill.ca

† tamipb@physics.mcgill.ca

‡ coish@physics.mcgill.ca

41]. Mook *et al.* [31] have shown that magnonic bands with this hybrid character can be topologically nontrivial in the presence of Dzyaloshinsky-Moriya interactions (DMI) [42, 43]. One of the systems considered in Ref. [31] is a square lattice of spins with an Ising anisotropy (an XXZ Heisenberg model) and DMI. This system can be mapped to a single-particle tight-binding problem on a Lieb lattice. The DMI is responsible for breaking an effective time-reversal symmetry (inducing an effective staggered flux in the Lieb lattice) and therefore allows the magnonic energy bands to be topologically nontrivial [31]. In this model, the presence of long-range (third-nearest-neighbor) interactions allows for the crossing of the single-magnon band with the TMBS. This crossing is needed to induce a topological phase transition. In this paper, we show that modulating the DMI in time is an alternative strategy to induce the band crossing and therefore to induce a topological phase transition, even in systems that may have very weak long-range spin couplings.

Originally proposed in electronic systems [44–46], the idea of using time-dependent fields to control the topological phase of a system (Floquet topological matter [47–49]) has also been applied to magnetic systems where the magnon number is conserved [50–53]. In addition to being motivated by the development of Floquet topological matter, our work is also motivated by recent advances in the post-growth control of the strength of the DMI [54, 55]. For example, it has been shown that the strength of the interfacial DMI can be modified and even change sign due to applied strain [56–58], applied electric fields [59–62], or by flipping the polarization of ferroelectric layers adjacent to the magnetic system [63]. These advances motivate us to investigate the possibility of inducing topologically nontrivial magnetic phases and to control them through a time-modulated DMI.

The rest of this paper is organized as follows. In Sec. II, we introduce the model, consisting of an XXZ Heisenberg Hamiltonian, a Zeeman field, and a periodically time-modulated DMI. In Sec. III, we review the low-energy excitations of the XXZ Hamiltonian, the presence of TMBSs in the case of Ising anisotropy, and the presence of an effective time-reversal symmetry that results in a topologically trivial magnon insulator. We also review the idea of hybrid magnons, i.e. eigenstates comprising a superposition of single-magnon and TMBSs hybridized by the DMI. In Sec. IV, we analyze the system with the time-modulated DMI. We obtain an effective time-independent Hamiltonian and study the topological properties (Chern numbers for the low-energy bands) and the associated conditions for the presence of robust edge modes. We show that in the case of a static DMI there are no edge modes present due to the absence of an energy gap and that this can be remediated by driving the DMI. Additionally, we show that the chirality of the edge states can be tuned by controlling a phase introduced between the time-modulated DMI acting between neighboring spins in the x and y directions (Sec. IV C) and

discuss the potential realization of our model (Sec. IV D). Finally, in Sec. V, we summarize our results.

II. MODEL

We consider a two-dimensional square lattice of spins [Fig. 1(a)] described by the time-dependent Hamiltonian

$$H(t) = H_S + H_{\text{DM}}(t), \quad (1)$$

where $H_{\text{DM}}(t)$ describes a time-dependent DMI and where H_S is a (static) XXZ Hamiltonian with a Zeeman field in the z direction (setting $\hbar = 1$):

$$H_S = \sum_{\langle \mathbf{r}, \mathbf{r}' \rangle} [-J_z S_{\mathbf{r}}^z S_{\mathbf{r}'}^z + J_{\perp} (S_{\mathbf{r}}^x S_{\mathbf{r}'}^x + S_{\mathbf{r}}^y S_{\mathbf{r}'}^y)] - B \sum_{\mathbf{r}} S_{\mathbf{r}}^z. \quad (2)$$

Here, $\mathbf{S}_{\mathbf{r}} = (S_{\mathbf{r}}^x, S_{\mathbf{r}}^y, S_{\mathbf{r}}^z)$ is the spin-1/2 operator associated with site \mathbf{r} , $J_z > 0$ is a ferromagnetic longitudinal coupling, and $J_{\perp} > 0$ is an antiferromagnetic transverse coupling. The signs of J_z and J_{\perp} will be important in what follows. The parameter B is the effective Zeeman field. The lattice consists of $N = L \times L$ sites so that the sum runs over $\mathbf{r} = n_x \mathbf{e}_x + n_y \mathbf{e}_y$, where $n_x, n_y = 1, \dots, L$ (setting the lattice constant $a = 1$), and where \mathbf{e}_i is the unit vector in the i direction.

The time-modulated DMI is assumed to take the form:

$$H_{\text{DM}}(t) = \sum_{\mathbf{r}} [D_x(t) (\mathbf{S}_{\mathbf{r}} \times \mathbf{S}_{\mathbf{r}+\mathbf{e}_x})_y + D_y(t) (\mathbf{S}_{\mathbf{r}} \times \mathbf{S}_{\mathbf{r}+\mathbf{e}_y})_x]. \quad (3)$$

We assume that the DMI can be modulated in time via, e.g., a symmetry-breaking time-dependent electric field or by inducing a time-dependent strain. In either case, it may be possible to independently control the strength of the DMI associated with nearest neighbors along x and y [$D_x(t) \neq D_y(t)$]. We will show in Sec. IV C, below, that this independent control can be used to change the chirality of the resulting topologically protected edge states. However, for most of this paper, we will restrict to the case where the two coupling parameters are equal and in-phase:

$$D_x(t) = D_y(t) = D(t) = D_0 + 2d \cos \omega t. \quad (4)$$

The DMI strength, $D(t)$, oscillates with amplitude $2d$ and frequency ω around the average value D_0 , making the Hamiltonian periodic $H(t+T) = H(t)$ with period $T = 2\pi/\omega$.

We work in the regime given by

$$J_z \gg J_{\perp}, D_0, \quad J_{\perp} \gg d. \quad (5)$$

The inequality $J_z \gg J_{\perp}, D_0$ guarantees a ferromagnetic ground state and allows us to treat both the transverse

terms and the DMI as a perturbation to the Ising Hamiltonian. Additionally, $J_z \gg J_\perp$ guarantees the presence of TMBSs as the energetic advantage of having two adjacent spin flips, J_z , separates these states from the two-magnon continuum, whose bandwidth scales with J_\perp [Fig. 1(b)]. The condition $J_\perp \gg d$ guarantees a weak off-resonant coupling between the TMBSs and the three-magnon states when driving the DMI; the detuning from resonance Δ [Fig. 1(b)] is of order J_\perp (see Sec. IV, below), while the coupling between the TMBSs and the three-magnon subspace is of order d .

Before continuing with the analytical treatment, we comment on the choice of an antiferromagnetic transverse coupling. For an antiferromagnetic coupling, the maximum of the single-magnon band coincides with the minimum of the TMBS bands at $\mathbf{k} = (0, 0)$ [Fig. 1(b)]. This admits a band inversion (via resonant driving), resulting in two Floquet bands with an energy gap that allows for the presence of robust edge states. For a ferromagnetic transverse coupling, the band minima of the magnon and TMBS bands would lie at the same point in the Brillouin zone. In this case, driving the DMI to induce the band crossing would not be a viable strategy in the regime given by Eq. (5), because the bands would overlap in energy whenever a level crossing could be induced.

In the next section, we review the ground state and low-energy excitations of the static Hamiltonian H_S and the effects of a static DMI [$D_0 \neq 0$, $d = 0$ in Eq. (3)]. Then, in Sec. IV we show how topologically protected Floquet edge states can be engineered by driving the DMI according to Eq. (4).

III. HYBRID MAGNONS

In this section we first review the single-magnon and two-magnon excitations of the XXZ Heisenberg model [Eq. (2)] and define the notation used in the rest of the paper (Secs. III A and III B). Then, in Sec. III C, we follow Ref. [31] and review how the single-magnon states are hybridized with the TMBSs via the DMI and how the effective time-reversal symmetry is broken, allowing these hybridized bands to be topologically nontrivial. Finally, we show that for a static DMI [$D_0 \neq 0$, $d = 0$ in Eq. (3)], the nontrivial bands overlap, hindering the presence of robust topologically-protected edge states.

A. Magnons

We first consider the ground state and low-energy excitations of the static Hamiltonian H_S . For a large Ising anisotropy, $J_z \gg J_\perp$, the XXZ Hamiltonian has a ferromagnetic ground state with every spin “up” ($S_r^z = +1/2$) when $B > 0$:

$$H_S |0\rangle = E_0 |0\rangle, \quad |0\rangle = |\uparrow, \dots, \uparrow\rangle, \quad (6)$$

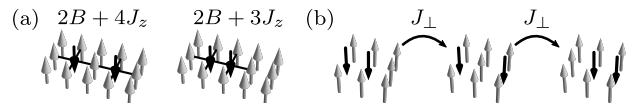


FIG. 2. (a) States with two spin flips and their associated energies in the Ising limit $J_\perp = 0$. (b) Hopping of a spin flip produced by the transverse exchange interactions in states with two spin flips.

with ground-state energy

$$E_0 = -\frac{1}{2}N(B + J_z). \quad (7)$$

Since H_S commutes with the z -component of total spin, $[H_S, \sum_{\mathbf{r}} S_{\mathbf{r}}^z] = 0$, it can be diagonalized in sectors having a definite number of spin flips. The lowest-energy excitations, composed of a linear combination of single spin flips, are the spin-wave (magnon) states $|\mathbf{k}\rangle$:

$$|\mathbf{k}\rangle = \frac{1}{\sqrt{N}} \sum_{\mathbf{r}} e^{i\mathbf{k}\cdot\mathbf{r}} |\mathbf{r}\rangle, \quad |\mathbf{r}\rangle \equiv S_{\mathbf{r}}^- |0\rangle, \quad (8)$$

where $|\mathbf{r}\rangle$ is the state with a spin flip at site \mathbf{r} and $S_{\mathbf{r}}^\pm = S_{\mathbf{r}}^x \pm iS_{\mathbf{r}}^y$ are the spin raising/lowering operators. The excitation energy (relative to E_0) of a magnon with wavevector \mathbf{k} is given by

$$E_{\mathbf{k}} = B + 2J_z + J_\perp (\cos k_x + \cos k_y). \quad (9)$$

Figure 1(b) shows the dispersion relation for the single-magnon states when $J_\perp = J_z/5$ and $B = 2J_z$. Since the static Hamiltonian conserves the number of spin flips, the single-magnon band is decoupled from the rest of the Hilbert space and it is always topologically trivial (a single band cannot have a nonzero Chern number).

B. Two-magnon bound states

After the single-magnon states, the states that are next highest in energy lie in the subspace of states with two spin flips,

$$|\mathbf{r}, \mathbf{r}'\rangle \equiv S_{\mathbf{r}}^- S_{\mathbf{r}'}^- |0\rangle. \quad (10)$$

To obtain the eigenstates of H_S in this subspace, we first consider the Ising limit ($J_\perp = 0$) and then treat the transverse coupling (term proportional to J_\perp) as a perturbation. In the Ising limit, the states $|\mathbf{r}, \mathbf{r}'\rangle$ are eigenstates with excitation energy $2B + 3J_z$ for adjacent spin flips and $2B + 4J_z$ otherwise. The energetic cost associated with non-adjacent spin flips (J_z) arises because adjacent spin flips have only six antiparallel nearest neighbors (instead of eight) [Fig. 2(a)]. The subspace with two spin flips is then separated into a low-energy sector composed of two-magnon bound states (TMBSs) ($|\mathbf{r}, \mathbf{r} + \mathbf{e}_x\rangle$ and $|\mathbf{r}, \mathbf{r} + \mathbf{e}_y\rangle$), and a high-energy sector composed of the states $|\mathbf{r}, \mathbf{r}'\rangle$ with $|\mathbf{r} - \mathbf{r}'| > 1$.

The transverse coupling induces hopping for spin flips and it couples the low-energy and high-energy sectors within the space of two spin flips, as it separates spin flips that are initially adjacent [Fig. 2(b)]. An effective Hamiltonian for the low-energy subspace can be obtained using second-order perturbation theory. The Hamiltonian contains the effective coupling between two low-energy states via a (higher-energy) virtual state as depicted in Fig. 2(b), where two actions of the perturbation results in an effective hopping from the state $|\mathbf{r}, \mathbf{r} + \mathbf{e}_x\rangle$ to the state $|\mathbf{r} + \mathbf{e}_x, \mathbf{r} + 2\mathbf{e}_x\rangle$.

Before writing down the effective Hamiltonian, we note that the Hamiltonian $H(t)$ has translational symmetry. Hence, it is convenient to Fourier transform the two-spin-flip states [Eq. (10)] with respect to the center point between the two spin-flip sites:

$$|\mathbf{k}, \mathbf{r}\rangle = \frac{1}{\sqrt{N}} \sum_{\mathbf{r}'} e^{i\mathbf{k}\cdot(\mathbf{r}'+\mathbf{r}/2)} |\mathbf{r}', \mathbf{r}' + \mathbf{r}\rangle. \quad (11)$$

The states above are not eigenstates of H_S , but the Hamiltonian preserves the wavevector \mathbf{k} : $\langle \mathbf{k}, \mathbf{r} | H_S | \mathbf{k}', \mathbf{r}' \rangle \propto \delta_{\mathbf{k}, \mathbf{k}'}$. This allows us to associate a wavevector to the two-magnon states and therefore to study their topological properties in terms of a Chern number, derived from effective Bloch states defined over the first Brillouin zone [37].

The TMBSs can be written in terms of the Fourier transforms [Eq. (11)] as

$$|\mathbf{k}, \mathbf{e}_x\rangle \equiv \frac{1}{\sqrt{N}} \sum_{\mathbf{r}} e^{i\mathbf{k}\cdot(\mathbf{r}+\mathbf{e}_x/2)} |\mathbf{r}, \mathbf{r} + \mathbf{e}_x\rangle, \quad (12)$$

$$|\mathbf{k}, \mathbf{e}_y\rangle \equiv \frac{1}{\sqrt{N}} \sum_{\mathbf{r}} e^{i\mathbf{k}\cdot(\mathbf{r}+\mathbf{e}_y/2)} |\mathbf{r}, \mathbf{r} + \mathbf{e}_y\rangle. \quad (13)$$

These states are coupled to the two-magnon continuum via the transverse coupling in H_S . When there is a large Ising anisotropy $J_z \gg J_\perp$, an effective Hamiltonian for the low-energy sector can be obtained using second-order perturbation theory (see Appendix B). Each block of the effective low-energy Hamiltonian, labeled by wavevector \mathbf{k} , is given by

$$h_{\mathbf{k}} = (2B + 3J_z) \sigma_0 - \frac{J_\perp^2}{J_z} \begin{pmatrix} c_x^2 + 2c_y^2 & 2c_x c_y \\ 2c_x c_y & 2c_x^2 + c_y^2 \end{pmatrix}, \quad (14)$$

in the basis $(|\mathbf{k}, \mathbf{e}_x\rangle, |\mathbf{k}, \mathbf{e}_y\rangle)^T$ where σ_0 is the 2×2 identity matrix, and we have used the abbreviation $c_i = \cos(k_i/2)$.

The Hamiltonian $h_{\mathbf{k}}$ is gapless at $\mathbf{k} = (\pi, \pi)$ and therefore it cannot have well defined Chern numbers, so it cannot host topologically protected edge states. More fundamentally, the Hamiltonian matrix elements $\langle \mathbf{k}, \mathbf{r} | H_S | \mathbf{k}, \mathbf{r}' \rangle$ are purely real [see Eq. (A1) in Appendix A], which means that H_S has an effective time-reversal symmetry (TRS), which prohibits the bands from having a non-zero Chern number. Although TRS is already broken in a system with magnetic ordering, it is the effective (and not the real) TRS that must be broken in

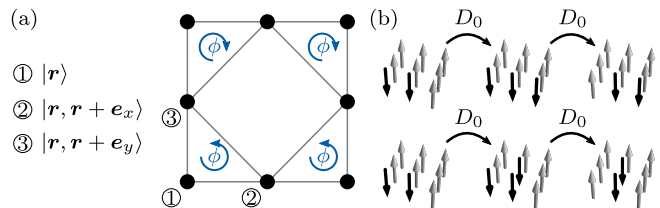


FIG. 3. (a) Effective Lieb lattice describing the low-energy subspace composed of single- and two-adjacent spin flips. The arrows indicate the direction in which the phase $\phi = \pi/2$ is acquired. (b) Some second-order processes contributing to matrix elements in Eq. (17). The virtual three-magnon states mediate an effective coupling between the TMBSs.

order to have non-zero Chern numbers. A Hamiltonian with translational symmetry described by the matrix $\mathcal{H}_{\mathbf{k}}$ has an effective TRS when $U^\dagger \mathcal{H}_{\mathbf{k}'} U = \mathcal{H}_{\mathbf{k}}^*$ is satisfied for a unitary transformation U and an orthogonal transformation of the momentum: $\mathbf{k}' = O\mathbf{k}$. In the presence of this symmetry, the Berry curvature has opposite signs at wavevectors \mathbf{k}, \mathbf{k}' and therefore the integrated Berry curvature over the BZ vanishes (see Appendix C). Since a real Hamiltonian satisfies $\mathcal{H}_{\mathbf{k}}^* = \mathcal{H}_{\mathbf{k}}$, it always has an effective TRS (in this case both U and O correspond to the identity operator).

In the next section, we show that although a static DMI ($D_0 \neq 0, d = 0$) breaks the effective TRS, its mere presence is not enough to obtain topologically protected edge states, as the absence of an energy gap may hinder their existence. However, we show that by driving the DMI ($d \neq 0$) we can obtain a (quasi-)energy gap that guarantees the presence of topologically protected edge states (Sec. IV).

C. Hybridized magnon bands

The DMI breaks rotational symmetry about the z -direction and it couples states having a number of spin flips that differs by one. The ferromagnetic ground state $|0\rangle$, remains an eigenstate, even in the presence of DMI as $H_{\text{DM}}(t)|0\rangle = 0$. In momentum space, the coupling between the single-magnon state and the TMBSs is given by

$$\langle \mathbf{k} | H_{\text{DM}}(t) | \mathbf{k}, \mathbf{e}_x \rangle = -iD(t)s_x, \quad (15)$$

$$\langle \mathbf{k} | H_{\text{DM}}(t) | \mathbf{k}, \mathbf{e}_y \rangle = D(t)s_y, \quad (16)$$

where $s_i = \sin(k_i/2)$. The DMI acts locally, coupling the single-magnon state only to the TMBSs (and not to the two-magnon continuum). The DMI also preserves translation symmetry and is therefore diagonal in momentum space.

In addition to coupling the single-magnon state and the TMBSs, the DMI breaks the effective TRS [31]. The breaking of the effective time-reversal symmetry can be understood by considering the low-energy subspace

spanned by the single-magnon state and the TMBSs, in real space: $\{|\mathbf{r}\rangle, |\mathbf{r}, \mathbf{r} + \mathbf{e}_x\rangle, |\mathbf{r}, \mathbf{r} + \mathbf{e}_y\rangle\}$. These states can be associated with the position of a particle hopping on a Lieb lattice, where the single spin flips correspond to the particle located at position \mathbf{r} and adjacent spin flips describe a particle located at the midpoint between the two spin flips, at $\mathbf{r} + \mathbf{e}_z/2$, as illustrated in Fig. 3(a). Without the DMI, the single-spin-flip states are decoupled from the two-adjacent spin-flip states. The DMI couples these states inducing an effective staggered flux, similar to the case of the Haldane model [21]. Here, as in the Haldane model, there is a nonzero local flux within part of a unit cell, but there is a net zero flux through the complete unit cell. The presence of this flux that cannot be gauged away can be understood from the matrix elements coupling the single spin flips and two-adjacent spin flips in the y -direction: $\langle \mathbf{r}, \mathbf{r} \pm \mathbf{e}_y | H_{\text{DM}}(t) | \mathbf{r} \rangle = \pm iD(t)/2$. Other hopping terms are real and don't contribute to the flux. The mapping of this problem to the Lieb lattice and the relationship to an effective time-reversal symmetry is also discussed at length in Ref. [31].

Before moving to the driven case, here we review the case, considered in Ref. [31], of a static DMI ($D_0 \neq 0$, $d = 0$) in the limit of large Ising anisotropy and weak DMI: $J_z \gg J_\perp, D_0$. Applying second-order perturbation theory in both the transverse exchange J_\perp and the DMI D_0 (Appendix B 2), the resultant low-energy Hamiltonian, now written in the basis $(|\mathbf{k}\rangle, |\mathbf{k}, \mathbf{e}_x\rangle, |\mathbf{k}, \mathbf{e}_y\rangle)^T$, is given by

$$H_{\mathbf{k}} = \begin{pmatrix} E_{\mathbf{k}} & -iD_0s_x & D_0s_y \\ iD_0s_x & E_{\mathbf{k}}^x & g_{\mathbf{k}} \\ D_0s_y & g_{\mathbf{k}}^* & E_{\mathbf{k}}^y \end{pmatrix}, \quad (17)$$

where

$$E_{\mathbf{k}}^x = 2B + 3J_z - \frac{J_\perp^2 (c_x^2 + 2c_y^2)}{J_z} - \frac{D_0^2 (2 - c_x^2)}{B + J_z}, \quad (18)$$

$$E_{\mathbf{k}}^y = 2B + 3J_z - \frac{J_\perp^2 (2c_x^2 + c_y^2)}{J_z} - \frac{D_0^2 (2 - c_y^2)}{B + J_z}, \quad (19)$$

$$g_{\mathbf{k}} = -2\frac{J_\perp^2}{J_z}c_xc_y - \frac{i}{2}\frac{D_0^2}{B + J_z}s_xs_y. \quad (20)$$

In addition to the coupling between the single magnon and the TMBSs, the TMBSs are coupled to the three-magnon states via the DMI. The three-magnon states mediate an effective second-order coupling between the TMBSs [see Fig. 3(b)].

Figure 4(a) shows the spectrum of Eq. (17) for $J_\perp = J_z/5$, $D_0 = J_z/15$, and $B = 2J_z$. The DMI produces a band opening at $\mathbf{k} = (\pi, \pi)$ and therefore the Chern numbers of the three bands are well defined and are given by $(0, 1, -1)$ from the lowest to the highest band. The Chern numbers are computed using the method by Fukui *et al.* [64] for a discrete Brillouin zone. To apply this method properly, the Hamiltonian $H_{\mathbf{k}}$ must be periodic in momentum space. To accomplish this,

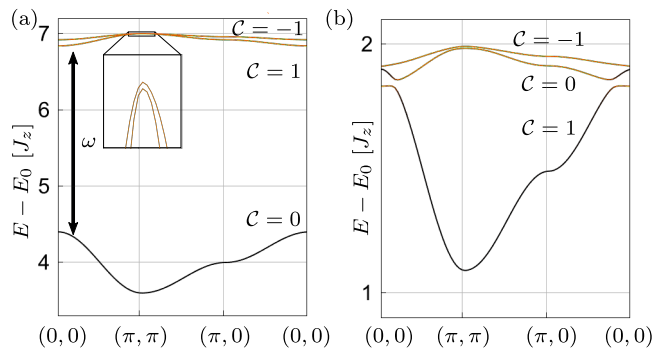


FIG. 4. (a) Bulk band structure with static DMI. In the undriven system, the Chern numbers are $(0, 1, -1)$. Driving the DMI with frequency ω resonantly couples the single-magnon band to the TMBS bands. (b) Bulk quasienergies of the Hamiltonian given by Eq. (24) (in the rotating frame). The color represents single-magnon (black) and TMBS character (orange/gray). The quasienergies for the system with open boundary conditions and the corresponding edge states are shown in Fig. 6.

we apply the unitary gauge transformation given by $U_{\mathbf{k}} = \text{diag}(1, e^{-ik_y/2}, e^{-ik_x/2})$.

The number of edge modes traversing an energy gap is given by the sum of the Chern numbers of the bands below this gap [23]. Since the lowest band has a zero Chern number, no edge modes are expected to traverse the energy gap between the lowest and the middle band. We would expect edge modes between the middle and highest bands if these were separated by an energy gap. This is not the case in the regime given by $J_\perp \gg D_0$. The lowest energy of the upper band is $2B + 3J_z - J_\perp^2/J_z$ for $\mathbf{k} = (0, 0)$ and is below the maximum energy of the middle band, given approximately by $\approx 2B + 3J_z - D_0^2/(B + J_z)$ at $\mathbf{k} = (\pi, \pi)$. The presence of topological edge states is therefore not guaranteed. This situation can be remediated by the presence of sufficiently strong next-nearest-neighbor interactions [31]. Here, however, we propose that in systems where these long-range interactions are too weak, time-modulating the DMI is an alternative strategy to produce edge modes.

IV. FLOQUET TOPOLOGICAL EDGE STATES

For weak DMI, $J_\perp \gg D_0$, the presence of robust edge modes is not guaranteed due to the absence of an energy gap between the topologically nontrivial bands. In this section, we show that topological magnon bands with an energy gap can be induced by driving the DMI. The goal is to produce a band inversion between the single-magnon band and the lower TMBS band by driving the DMI with a frequency that compensates for this gap [Fig. 4(a)].

A. Floquet bands

The topological properties of a periodic Hamiltonian with period T : $H(t+T) = H(t)$ can be studied in terms of its Floquet states. The Floquet states $\{|\psi_\alpha(t)\rangle\}$ form a set of orthogonal solutions to the time-dependent Schrödinger equation $i\frac{d}{dt}|\psi_\alpha(t)\rangle = H(t)|\psi_\alpha(t)\rangle$ (setting $\hbar = 1$). These solutions have the form $|\psi_\alpha(t)\rangle = e^{-i\varepsilon_\alpha t}|\phi_\alpha(t)\rangle$, where $|\phi_\alpha(t)\rangle$ has the same periodicity as the Hamiltonian: $|\phi_\alpha(t+T)\rangle = |\phi_\alpha(t)\rangle$ and ε_α is known as the quasienergy [47, 48]. At stroboscopic times $t = nT$, the Floquet state is periodic up to a phase that is proportional to the quasienergy, $|\psi_\alpha(nT)\rangle = e^{-i\varepsilon_\alpha nT}|\psi_\alpha(0)\rangle$, as would be true for an eigenstate evolving under a time-independent Hamiltonian with energy ε_α . The state $|\psi_\alpha(0)\rangle$ is then the eigenstate of a time-independent Hamiltonian, the Floquet Hamiltonian H_F , defined by the time-evolution operator over one period:

$$U(T, 0) = \mathcal{T}e^{-i\int_0^T dt' H(t')} \equiv e^{-iH_F T}, \quad (21)$$

where \mathcal{T} is the time-ordering operator [47, 48]. The topological properties of the time-dependent Hamiltonian $H(t)$ can then be studied using the Floquet states $|\psi_\alpha(0)\rangle$.

To obtain the Floquet states we go into a rotating frame given by $|\psi(t)\rangle = U(t)|\tilde{\psi}(t)\rangle$ where $U(t) = \exp(-i\omega S_{\text{sf}} t)$, where $S_{\text{sf}} = N/2 - \sum_{\mathbf{r}} S_{\mathbf{r}}^z$ counts the number of spin flips. The Hamiltonian in the rotating frame is given by

$$\begin{aligned} \tilde{H}(t) &= U^\dagger(t)H(t)U(t) - iU^\dagger(t)\dot{U}(t) \\ &= U^\dagger(t)H(t)U(t) - \omega S_{\text{sf}} \\ &= H_S + U^\dagger(t)H_{\text{DM}}(t)U(t) - \omega S_{\text{sf}}. \end{aligned} \quad (22)$$

The static Hamiltonian H_S commutes with S_{sf} (as it preserves the number of spin flips) and hence it is unaffected by the unitary transformation. The last term in Eq. (22) shifts the n -magnon band down in energy by $n\omega$, reducing the spacing between pairs of bands associated with a different number of magnons. The second term in Eq. (22) includes a time-independent DMI with amplitude d , and fast oscillating DMI terms [with amplitudes D_0 and d , cf. (B7) in Appendix B3]. These terms can be neglected using the rotating-wave approximation (RWA) in the regime given by $d, D_0 \ll J_z$. Then, in the rotating frame the Hamiltonian can be approximated by

$$\begin{aligned} \tilde{H} &\approx H_S - \omega S_{\text{sf}} \\ &+ d \sum_{\mathbf{r}} [(\mathbf{S}_{\mathbf{r}} \times \mathbf{S}_{\mathbf{r}+\mathbf{e}_x})_y + (\mathbf{S}_{\mathbf{r}} \times \mathbf{S}_{\mathbf{r}+\mathbf{e}_y})_x]. \end{aligned} \quad (23)$$

Here, as in Sec. III C, we apply second-order perturbation theory in the transverse exchange J_\perp and the DMI (now with amplitude d), valid in the regime $d \ll J_\perp$, $J_\perp \ll J_z$, and obtain the effective Hamiltonian in momentum space

$$\tilde{H}_{\mathbf{k}} = \begin{pmatrix} E_{\mathbf{k}} - \omega & -ids_x & ds_y \\ ids_x & \tilde{E}_{\mathbf{k}}^x - 2\omega & \tilde{g}_{\mathbf{k}} \\ ds_y & \tilde{g}_{\mathbf{k}}^* & \tilde{E}_{\mathbf{k}}^y - 2\omega \end{pmatrix}, \quad (24)$$

where

$$\tilde{E}_{\mathbf{k}}^x = 2B + 3J_z - \frac{J_\perp^2 (c_x^2 + 2c_y^2)}{J_z} - \frac{d^2 (2 - c_x^2)}{B + J_z - \omega}, \quad (25)$$

$$\tilde{E}_{\mathbf{k}}^y = 2B + 3J_z - \frac{J_\perp^2 (c_y^2 + 2c_x^2)}{J_z} - \frac{d^2 (2 - c_y^2)}{B + J_z - \omega}, \quad (26)$$

$$\tilde{g}_{\mathbf{k}} = -\frac{2J_\perp^2}{J_z} c_x c_y - i \frac{d^2}{B + J_z - \omega} s_x s_y. \quad (27)$$

Note that, since the transformation to the rotating frame through $U(t)$ preserves the number of spin-flip excitations, the Floquet states remain in a superposition of states with different magnon number even when the Floquet states are nonstationary when rewritten in the lab frame.

After comparing with the effective Hamiltonian for the case of static DMI, Eq. (17), we observe two main differences. First, the spacing between the single-magnon band and the TMBS band is reduced by ω . Second, there is a modification of the second-order corrections (terms proportional to d^2) coming from coupling to the three-magnon states. This is because the three-magnon states are also shifted by an amount ω closer to the TMBS bands.

A topological phase transition might occur if the gap between the single-magnon band and the TMBS bands closes. This occurs when ω is greater than the energy gap:

$$\omega > B + J_z - 2J_\perp - \frac{5J_\perp^2}{J_z}. \quad (28)$$

The band gap of the undriven system H_S , given by the RHS of the inequality above, is the energy difference between the lowest energy of the TMBS bands and the highest point of the single-magnon band, both located at $\mathbf{k} = (0, 0)$ and given by $2B + 3J_z - 5J_\perp^2/J_z$ and $B + 2J_z + 2J_\perp$ (up to second-order corrections in J_\perp), respectively. In this range of frequencies, the single-magnon band is shifted up in energy, crossing the lowest TMBS band and the bands undergo a topological phase transition. Figure 4(b) shows an example for $J_\perp = J_z/5$, $B = 2J_z$, $D = J_z/15$, $\lambda = 1$, and $\omega = 2.5J_z$. The Chern number of the lowest band goes from 0 to 1 and the Chern number of the middle band goes from 1 to 0. The bands have both single-magnon and TMBS character (see color scale). Contrary to the static case, there is an energy gap between the lower band and the middle band, allowing for the presence of robust edge modes.

To induce a band inversion that guarantees the presence of topologically protected edge states, the driving frequency ω must be larger than the lower bound [Eq. (28)]. As we increase the frequency, the TMBSs will eventually become resonantly coupled to the three-magnon states. This sets an upper bound for ω as our perturbative approach is valid only if the detuning Δ between the TMBSs and the three-magnon states is large compared to the amplitude of the oscillating DMI d . This

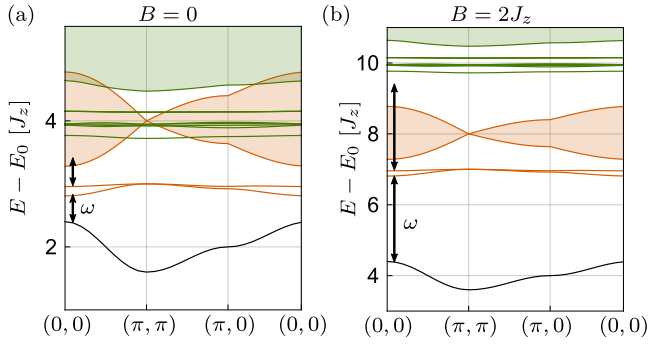


FIG. 5. Exact diagonalization of the static Hamiltonian H_S with $J_{\perp} = J_z/5$ and two values of the magnetic field B . (a) In the absence of a magnetic field ($B = 0$), the frequency ω required to resonantly couple the single-magnon and TMBS bands also resonantly couples the TMBSs to the two-magnon continuum. (b) A magnetic field B can be used to avoid these undesired resonances.

upper bound is the energy difference between the lowest three-magnon state, given by $3B + 4J_z - J_{\perp}$ (Appendix D), and the highest energy of the TMBSs, given by $2B + 3J_z$. The detuning is

$$\Delta = B + J_z - J_{\perp} - \omega. \quad (29)$$

Our perturbative approach is then valid when $\Delta \gg d$. The detuning must be positive to avoid coupling the TMBSs to higher-energy three-magnon states. This means that

$$\omega < B + J_z - J_{\perp} \quad (30)$$

must be satisfied. This condition together with Eq. (28) result in

$$0 < J_{\perp} - \Delta < J_{\perp}. \quad (31)$$

Therefore, the detuning Δ is at most of order J_{\perp} . Aiming to maximize the quasi-energy gap, which is of order d , means driving with a frequency that is close to this maximal value for the detuning, i.e. $\Delta \sim J_{\perp}$. In this regime, our perturbative approach is valid when $J_{\perp} \gg d$.

The magnetic field B does not play a role in the equations describing the regime of validity of our perturbative analysis and is not necessary for the physics discussed above. This is because the magnetic field increases the energy separation between magnon bands with different magnon number [Fig. 5]. To produce the resonant coupling between the single-magnon and the TMBS bands, this energy difference must be overcome [Eq. (28)]. This is explicit in the diagonal matrix elements of Eq. (24). Every term containing B has at least one $-\omega$ term. Nevertheless, the magnetic field can be used as a handle to avoid resonances between the TMBSs and the two-magnon continuum in the case where the mechanism used to time-modulate the DMI (e.g. electric fields or strain) produce an unintended modulation of the exchange parameter J_{\perp} (see Fig. 5).

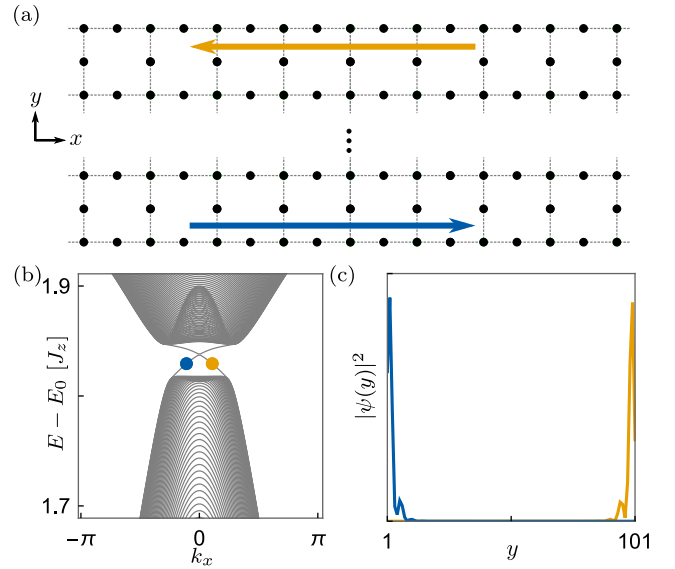


FIG. 6. (a) Effective Lieb lattice with open boundary conditions in the y direction and periodic boundary conditions in the x direction. (b) Spectrum of the system with open boundary conditions in the y direction. The (normalized) wavefunctions associated with the k_x points indicated with circles are shown in (c). The parameters used in this plot are $J_{\perp} = J_z/5$, $B = 2J_z$, $\omega = 2.5J_z$, $d = J_z/15$.

B. Edge states

To verify the presence of edge states we work in a ribbon geometry with periodic boundary conditions in the x direction and open boundary conditions in y [see Fig. 6(a)]. We use the partial Fourier transform

$$|\psi_{\mathbf{k}}\rangle = \frac{1}{\sqrt{L}} \sum_y e^{ik_y y} U_{k_y}^{\dagger} |\psi_{k_x y}\rangle, \quad (32)$$

where $|\psi_{\mathbf{k}}\rangle = (|\mathbf{k}\rangle, |\mathbf{k}, \mathbf{e}_x\rangle, |\mathbf{k}, \mathbf{e}_y\rangle)^T$ is our basis vector in momentum space and $U_{k_y}^{\dagger} = \text{diag}(1, 1, e^{ik_y/2})$ ensures the Fourier transform is taken with respect to the position of each site in the Lieb lattice [staying consistent with Eq. (13)]. The Hamiltonian for the ribbon is straightforwardly obtained by using Eq. (32) in Eq. (24) and is given in Appendix E [Eq. (E3)]. In the ribbon geometry considered here, the Lieb lattice terminates in a row containing single-spin-flip states $|n_x \hat{x} + L \hat{y}\rangle$ and two adjacent spin flips in the x -direction $|n_x \hat{x} + L \hat{y}, \hat{y}\rangle$ [see Fig. 6(a)]. The state $|n_x \hat{x} + L \hat{x}, \hat{y}\rangle$ does not exist because it would correspond to flipping the spins at positions (n_x, L) and $(n_x, L+1)$, which is outside the system boundary.

Figure 6(b) shows the spectrum of the system with the ribbon geometry for $B = 2J_z$, $J_{\perp} = J_z/5$, $d = J_z/15$, $\omega = 2.5J_z$. Although the bulk spectrum is fully gapped, the ribbon supports counter-propagating edge modes that traverse the bulk gap between the lowest and middle band (Fig. 6). These edge modes are protected against

perturbations that do not close the quasi-energy gap [9] which, in our system, is given by the amplitude of the modulation of the DMI d .

In Floquet topological systems, anomalous edge modes traversing energy gaps between bands with trivial Chern numbers can appear, differentiating the topological bulk-boundary correspondence of systems in equilibrium [46, 47, 65]. These states may appear in systems where the minimum of the lowest-energy band and the maximum of the highest-energy band touch resulting in a band closure and reopening (this is allowed in Floquet systems because the quasienergy spectrum is periodic in energy) [65]. In our system and in the regime under consideration: $J_{\perp} \ll J_z$, the frequency ω [of order J_z , cf. Eq. (28)] is larger than the bandwidths [of order J_{\perp} , cf. Eq. (24) and (29)] and the aforementioned gap closing and reopening will not occur. Hence, there will be no anomalous edge modes in the regime under consideration.

C. Controlling chirality

We now consider the case in which the DMI can be independently time-modulated for spins that are nearest neighbors along the x and y directions, $D_x(t) \neq D_y(t)$ [see Eq. (3)]. We focus on the case where the amplitude and frequency of the drive are the same but there is a phase difference φ between them:

$$D_x(t) = D_0 + 2d \cos(\omega t + \varphi), \quad (33)$$

$$D_y(t) = D_0 + 2d \cos(\omega t). \quad (34)$$

Going through the same procedure used to obtain Eq. (24), the effective Hamiltonian in the rotating frame is given by

$$\tilde{H}'_{\mathbf{k}} = \begin{pmatrix} E_{\mathbf{k}} - \omega & -ie^{-i\varphi} ds_x & ds_y \\ ie^{i\varphi} ds_x & \tilde{E}_{\mathbf{k}}^x - 2\omega & g'_{\mathbf{k}} \\ ds_y & (\tilde{g}'_{\mathbf{k}})^* & \tilde{E}_{\mathbf{k}}^y - 2\omega \end{pmatrix}, \quad (35)$$

where

$$\tilde{g}'_{\mathbf{k}} = -2 \frac{J_{\perp}^2}{J_z} c_x c_y - \frac{i}{2} \frac{d^2}{B + J_z - \omega} e^{i\varphi} s_x s_y. \quad (36)$$

The phase φ can then be used to tune the topological phase and hence the propagation direction of the magnon edge states. Figure 7 shows the Chern numbers for the three bands of the Hamiltonian (35) as a function of φ and the insets show the chirality of the edge states in the different topological phases. The Chern numbers are computed using the method by Fukui *et al.*, as in the previous sections. The phase transition caused by the variation of φ can be understood by comparing the Hamiltonians obtained for φ and $\varphi + \pi$. These Hamiltonians are related by complex conjugation: $\tilde{H}'_{\mathbf{k}}(\varphi) = [\tilde{H}'_{\mathbf{k}}(\varphi + \pi)]^*$ which means that they are related by an effective time-reversal (TR) operation. This operation consists of the real TR and a rotation of the spin operators by π about

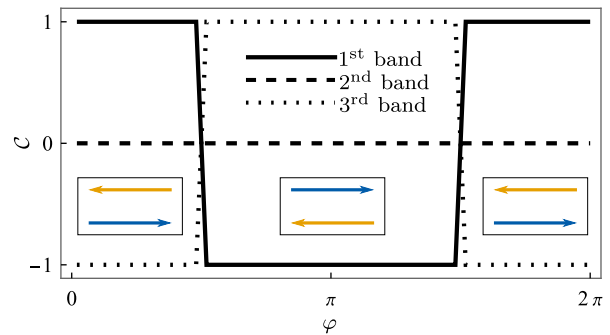


FIG. 7. Chern numbers as a function of the relative phase φ between the time-modulation of the DMI between neighboring spins in the x and y directions [see Eqs. (33) and (34)]. The inset show the direction of the topological edge states. The parameters used for this plot are $J_{\perp} = J_z/5$, $B = 2J_z$, $\omega = 2.5J_z$, $d = J_z/15$.

the x or y axis, as shown by Mook *et al.* [31]. As a consequence of this relation, the Berry curvatures of the eigenstates of $\tilde{H}'_{\mathbf{k}}(\varphi)$ and $\tilde{H}'_{\mathbf{k}}(\varphi + \pi)$ have opposite sign (see Appendix C 2) and therefore their corresponding Chern numbers also have opposite sign (Fig. 7). This sign change of the Chern number results in the reversal of the chirality of the edge modes [23].

D. Potential experimental realization

By proposing the time modulation of the DMI, we extend the range of materials in which magnonic topological edge modes having single-magnon and two-magnon character can be found by removing the necessity of exchange interactions beyond nearest neighbors [31]. Here, we have used a simple model to illustrate how driving the DMI may induce a topological phase transition. The idea of driving the DMI to induce topological phase transitions may be applied to other lattices and different spin S . Systems with $S > 1/2$ may allow for the existence of a different type of bound state, the *single-ion bound state*, in the presence of single-ion anisotropy [31, 40].

Van der Waals magnets [66–68] are one class of two-dimensional materials that may be suitable for the implementation of the technique proposed here. Easy-axis anisotropy (Ising and/or single-ion) has been found, for example, in $\text{Cr}_2\text{Ge}_2\text{Te}_6$ [69] and CrI_3 [70, 71]. Another set of interesting materials includes Janus monolayers [72, 73] which may have Ising or single-ion anisotropy and where inversion symmetry is inherently broken allowing for the DMI considered here [74–76]. Both van der Waals magnets and Janus monolayers [69, 70, 74–76] have exchange couplings on the order of meV and therefore the frequency ω [which is on the order of $B + J_z$, cf. Eqs. (29) and (31)] required for resonant driving lies in the THz regime. One strategy to drive the DMI is therefore the use of a THz-frequency electric field. In van der Waals materials, it has been predicted that the

DMI amplitude depends linearly on an externally applied static electric field and the strength of the DMI can be changed by up to ~ 1 meV using field amplitudes of $E \sim 1$ V/nm [62]. An oscillating electric field may then be used to drive the DMI [Eq. (4)] if the drive adiabatically modulates the magnetic system without generating spurious excitations. The THz radiation will also generate a direct magnetic coupling, which could resonantly couple the single-magnon state to the TMBSs. This coupling, given by $\langle \mathbf{k} | \mu \mathbf{B}_\perp \cdot \mathbf{S}_\perp | \mathbf{k}, \mathbf{e}_i \rangle = \mu |\mathbf{B}_\perp| \cos(k_i/2)$ (μ is the magnetic moment of the magnetic atom and \mathbf{B}_\perp , \mathbf{S}_\perp are the in-plane components of the magnetic field and spin operator) in the rotating frame, will not affect the topological phase of the system when its strength is small compared to the quasienergy gap of order d : $\mu |\mathbf{B}_\perp| \ll d$. The amplitude of the DMI can also be changed by up to ~ 1 meV by varying the polarization of ferroelectric layers in van der Waals heterostructures [63] or by applying strain [57]. Modulation of the polarization in ferroelectrics [77–79] and strain [80, 81] in the THz regime has been achieved experimentally and can serve as additional strategies to drive the DMI. Furthermore, since the DMI depends on the same orbital overlaps as Heisenberg exchange, lattice vibrations that modulate the Heisenberg exchange interaction in the THz regime [82,83] are also expected to modulate the DMI in this frequency range (spurious resonances that may occur when modulating the other exchange parameters can be prevented by changing the value of an external magnetic field, see Fig. 5). We note that, although the materials mentioned above ($\text{Cr}_2\text{Ge}_2\text{Te}_6$, CrI_3 , Janus monolayers of manganese dichalcogenides, VSeTe and $\text{Cr}(\text{I}, \text{X})_3$) have easy-axis anisotropy (Ising and/or single-ion), the condition $J_\perp \ll J_z$ is not satisfied in any of them and therefore this list does not contain a direct candidate material. However, the discovery of new van der Waals magnets is an active field of research [66] which may lead to materials with stronger anisotropy to satisfy the condition $J_\perp \ll J_z$.

A more direct implementation could be realized using Rydberg atoms which can be used to simulate magnetic systems [82]. By applying a sequence of global and local pulses, it is possible to engineer the XXZ Hamiltonian with the DMI interactions of our model. The strength of the magnetic interactions depends on the time interval between the applied pulses which can be varied to generate the time-modulation of the DMI [83]. Systems of cold atoms, also used to simulate magnetic systems are an additional alternative to simulate the physics proposed in this paper. In these systems, in addition to XXZ anisotropy [84, 85], a synthetic spin-orbit interaction can be engineered resulting in an effective spin Hamiltonian with DMI [86–88].

V. CONCLUSION

We have shown that a periodic modulation of the DMI can be used as a strategy to produce robust topological edge modes in quantum magnets. We considered the case of a square lattice of spins with ferromagnetic longitudinal interactions, antiferromagnetic transverse interactions, and DMI. In the case of a static DMI, the magnonic system is topologically non-trivial in the sense that the bands have nonzero Chern numbers. However, robust edge modes are absent due to the lack of an energy gap between the non-trivial bands in the regime under consideration: $J_z \gg J, D_0$. We have further shown that, by driving the DMI, a band inversion between the single-magnon band and the TMBSs is produced with an energy gap that allows for the existence of robust edge states. Furthermore, we have shown that the chirality of the edge states can be controlled by driving the DMI for neighbors in the x and y direction with a relative phase.

ACKNOWLEDGMENTS

We acknowledge support from Fonds de Recherche du Québec–Nature et Technologies (FRQNT). TP-B and WAC acknowledge support from Natural Sciences and Engineering Research Council of Canada (NSERC) and Institut Transdisciplinaire d’Information Quantique (INTRIQ). TP-B acknowledges the hospitality of the Institut de Ciències Fotoniques (Barcelona) where some of the work took place.

Appendix A: Exact diagonalization of the static Hamiltonian

Figure 1(b) shows the spectrum of the static Hamiltonian H_S in the subspaces of one, two, and three spin flips. H_S preserves the number of spin flips and it can be diagonalized in subspaces with a definite number of spin flips. For one spin flip, there is only the single-magnon band given by Eq. (9).

To obtain the spectrum of the two-magnon states, we first need to choose a basis. Since we have translation symmetry we use the two-magnon states $|\mathbf{k}, \mathbf{r}\rangle$ defined in Eq. (11). The matrix elements are obtained by applying H_S to $|\mathbf{k}, \mathbf{r}\rangle$:

$$H_S |\mathbf{k}, \mathbf{r}\rangle = \left(2B + 4J_z - J_z \sum_{i=x,y} \delta_{\mathbf{r}, \mathbf{e}_i} \right) |\mathbf{k}, \mathbf{r}\rangle + J_\perp \sum_{\substack{i=x,y \\ \sigma=\pm}} \cos \frac{k_i}{2} |\mathbf{k}, \mathbf{r} + \sigma \mathbf{e}_i\rangle. \quad (\text{A1})$$

The state $|\mathbf{k}, \mathbf{r}\rangle$ is a superposition of the states with two spin flips separated by $\mathbf{r} = n_x \mathbf{e}_x + n_y \mathbf{e}_y$ [cf. Eq. (11)] (where $n_x, n_y \geq 0$ are defined modulo L). For spin $1/2$,

$n_x, n_y = 0$ is not an option as this corresponds to applying the spin lowering operator twice on the same lattice site. Furthermore, from the remaining $N - 1$ vectors satisfying $(n_x, n_y) \neq (0, 0)$, the states $|\mathbf{k}, \mathbf{r}\rangle$ and $|\mathbf{k}, L\mathbf{e}_x + L\mathbf{e}_y - \mathbf{r}\rangle$ are the same [cf. Eq. (11)]. For odd L , this means that each of the N wavevectors \mathbf{k} has $(N - 1)/2$ options for \mathbf{r} so that the size of the Hilbert space of the two-magnon states is $N(N - 1)/2$, the number of ways in which two spins can be flipped. For even L , the vectors $\mathbf{r} \in \{L/2\mathbf{e}_x, L/2\mathbf{e}_y, L/2\mathbf{e}_x + L/2\mathbf{e}_y\}$ are the same as $L\mathbf{e}_x + L\mathbf{e}_y - \mathbf{r}$ and for these vectors there are only $N/2$ distinct wavevectors \mathbf{k} that give distinct $|\mathbf{k}, \mathbf{r}\rangle$. Hence, for even L , there are 3 vectors \mathbf{r} that have $N/2$ options for \mathbf{k} and $(N - 4)/2$ vectors \mathbf{r} that have N

choices of \mathbf{k} , so that the size of the Hilbert space is again $N(N - 1)/2$. Figure 1(b) shows the spectrum for $L = 7$.

To obtain the spectrum of the three-magnon states we use the basis

$$|\mathbf{k}, \mathbf{r}_1, \mathbf{r}_2\rangle = \frac{1}{\sqrt{N}} \sum_{\mathbf{r}} e^{i\mathbf{k}\cdot(\mathbf{r} + \frac{\mathbf{r}_1 + \mathbf{r}_2}{3})} |\mathbf{r}, \mathbf{r} + \mathbf{r}_1, \mathbf{r} + \mathbf{r}_2\rangle, \quad (\text{A2})$$

where

$$|\mathbf{r}, \mathbf{r}', \mathbf{r}''\rangle \equiv S_{\mathbf{r}}^- S_{\mathbf{r}'}^- S_{\mathbf{r}''}^- |0\rangle. \quad (\text{A3})$$

The matrix elements can be obtained by applying H_S on Eq. (A2):

$$H_S |\mathbf{k}, \mathbf{r}_1, \mathbf{r}_2\rangle = \left[3B + 6J_z - J_z \sum_i (\delta_{\mathbf{r}_1, \mathbf{e}_i} + \delta_{\mathbf{r}_2, \mathbf{e}_i} + \delta_{\mathbf{r}_1 - \mathbf{r}_2, \mathbf{e}_i}) \right] |\mathbf{k}, \mathbf{r}_1, \mathbf{r}_2\rangle + J_{\perp} \sum_{\substack{i=x,y \\ \sigma=\pm}} e^{-i\sigma k_i/3} (|\mathbf{k}, \mathbf{r}_1 - \sigma\mathbf{e}_i, \mathbf{r}_2 - \sigma\mathbf{e}_i\rangle + |\mathbf{k}, \mathbf{r}_1 + \sigma\mathbf{e}_i, \mathbf{r}_2\rangle + |\mathbf{k}, \mathbf{r}_1, \mathbf{r}_2 + \sigma\mathbf{e}_i\rangle). \quad (\text{A4})$$

The states $|\mathbf{k}, \mathbf{r}_1, \mathbf{r}_2\rangle$, $|\mathbf{k}, -\mathbf{r}_1, \mathbf{r}_2 - \mathbf{r}_1\rangle$, and $|\mathbf{k}, -\mathbf{r}_2, \mathbf{r}_1 - \mathbf{r}_2\rangle$ are the same [cf. Eq. (A2)]. Hence, the size of the Hilbert subspace for each wavevector \mathbf{k} is $(N - 1)(N - 2)/6$.

Appendix B: Effective Hamiltonians

1. Perturbation theory

For a time-independent Hamiltonian given by

$$H = H_0 + V, \quad H_0 |\alpha\rangle = \varepsilon_{\alpha} |\alpha\rangle, \quad (\text{B1})$$

where the eigenvalues ε_{α} and eigenstates $|\alpha\rangle$ of H_0 are known, an effective Hamiltonian describing the low-energy subspace can be obtained using perturbation theory. The matrix elements of this effective Hamiltonian, up to second-order corrections in V , are given by (see, for example, complement BI of Ref. [89])

$$H_{\alpha\beta}^{\text{eff}} = (H_0 + V)_{\alpha\beta} + \frac{1}{2} \sum_{\gamma} V_{\alpha\gamma} V_{\gamma\beta} \left(\frac{1}{\varepsilon_{\alpha} - \varepsilon_{\gamma}} + \frac{1}{\varepsilon_{\beta} - \varepsilon_{\gamma}} \right), \quad (\text{B2})$$

where the indices $\alpha\beta$ label states in the low-energy subspace and γ are higher-energy states out of the low-energy subspace of interest.

2. Effective Hamiltonian in the static case

To obtain the Hamiltonians (14) and (17) corresponding, respectively, to the case of vanishing DMI ($D = 0, d = 0$) and the case of time-independent DMI ($d = 0$). We take the Ising part of $H(t)$ as the unperturbed Hamiltonian and the transverse exchange interactions and the DMI as perturbations. In the the case of a static DMI the Hamiltonian $H(t)$ becomes time independent:

$$H(t) \rightarrow H = H_0 + V_1 + V_2, \quad (\text{B3a})$$

where

$$H_0 = -J_z \sum_{\langle \mathbf{r}, \mathbf{r}' \rangle} S_{\mathbf{r}}^z S_{\mathbf{r}'}^z - B \sum_{\mathbf{r}} S_{\mathbf{r}}^z, \quad (\text{B3b})$$

$$V_1 = J_{\perp} \sum_{\langle \mathbf{r}, \mathbf{r}' \rangle} (S_{\mathbf{r}}^x S_{\mathbf{r}'}^x + S_{\mathbf{r}}^y S_{\mathbf{r}'}^y), \quad (\text{B3c})$$

$$V_2 = D_0 \sum_{\mathbf{r}} [(S_{\mathbf{r}} \times S_{\mathbf{r} + \mathbf{e}_x})_y + (S_{\mathbf{r}} \times S_{\mathbf{r} + \mathbf{e}_y})_x]. \quad (\text{B3d})$$

The treatment of V_1, V_2 as perturbations is justified in the limit

$$J_z \gg J, D_0, \quad (\text{B4})$$

as the energy difference between the low-energy subspace $\{|\mathbf{k}\rangle, |\mathbf{k}, \mathbf{e}_x\rangle, |\mathbf{k}, \mathbf{e}_y\rangle\}$ and the (higher-energy) states coupled to it by V_1, V_2 is at least J_z . To obtain Eqs. (14) and (17) we use Eq. (B2) with $V = V_1$ and $V = V_1 + V_2$, respectively.

3. Effective Hamiltonian with time-dependent DMI

To obtain the effective Hamiltonian in the case of the time-modulated DMI, we go into a rotating frame given by $|\psi(t)\rangle = U(t)|\tilde{\psi}(t)\rangle$ where

$$U(t) = e^{-i\omega S_{\text{sf}}t}, \quad S_{\text{sf}} = \frac{N}{2} - \sum_{\mathbf{r}} S_{\mathbf{r}}^z, \quad (\text{B5})$$

where S_{sf} counts the number of spin flips. The Hamiltonian dictating the time-evolution of the states $|\tilde{\psi}(t)\rangle$ in

$$\begin{aligned} U^\dagger(t)H_{\text{DM}}(t)U(t) &= e^{i\omega S_{\text{sf}}t} (D_0 + de^{i\omega t} + de^{-i\omega t}) \sum_{\mathbf{r}} [(\mathbf{S}_{\mathbf{r}} \times \mathbf{S}_{\mathbf{r}+\mathbf{e}_x})_y + (\mathbf{S}_{\mathbf{r}} \times \mathbf{S}_{\mathbf{r}+\mathbf{e}_y})_x] e^{-i\omega S_{\text{sf}}t} \\ &= \sum_n \left\{ P_n \left[(e^{-i\omega t} D_0 + d + de^{-2i\omega t}) \sum_{\mathbf{r}} [(\mathbf{S}_{\mathbf{r}} \times \mathbf{S}_{\mathbf{r}+\mathbf{e}_x})_y + (\mathbf{S}_{\mathbf{r}} \times \mathbf{S}_{\mathbf{r}+\mathbf{e}_y})_x] \right] P_{n+1} + \text{h.c.} \right\}. \end{aligned} \quad (\text{B7})$$

As explained in the main text we focus on the regime where the single magnon band is resonantly coupled to the TMBSs and the TMBSs is off-resonant from the three-magnon states [see Fig. 1(b)]. Neglecting counter-rotating terms, we have

$$U^\dagger(t)H_{\text{DM}}(t)U(t) \approx d \sum_{\mathbf{r}} [(\mathbf{S}_{\mathbf{r}} \times \mathbf{S}_{\mathbf{r}+\mathbf{e}_x})_y + (\mathbf{S}_{\mathbf{r}} \times \mathbf{S}_{\mathbf{r}+\mathbf{e}_y})_x] \quad (\text{B8})$$

The Hamiltonian in the rotating frame then is the same as the Hamiltonian with static DMI, now with strength d instead of D_0 , and where the n -magnon bands are shifted $n\omega$ downwards in energy, bringing bands with different number of magnons closer to each other. We then apply the same perturbative approach as we did to obtain the effective Hamiltonian for the static DMI to obtain Eq. (24). In the case where a phase between the DMI in the x and y directions [$D_x(t) \neq D_y(t)$] is present the DMI in the rotating-wave approximation is given by

$$\begin{aligned} U^\dagger(t)H'_{\text{DM}}U(t) &\approx d \sum_{\mathbf{r}} (\mathbf{S}_{\mathbf{r}} \times \mathbf{S}_{\mathbf{r}+\mathbf{e}_y})_x \\ &+ d \sum_{rn} [e^{i\varphi} P_n (\mathbf{S}_{\mathbf{r}} \times \mathbf{S}_{\mathbf{r}+\mathbf{e}_x})_y P_{n+1} + \text{h.c.}], \end{aligned} \quad (\text{B9})$$

which can be seen from adding the corresponding phase in Eq. (B7).

Appendix C: Chern numbers and effective time-reversal symmetry

1. Berry curvature

The topology of a two-dimensional system without symmetry restrictions, other than translation symmetry,

the rotating frame is given by

$$\begin{aligned} \tilde{H}(t) &= U^\dagger(t)H(t)U(t) - \omega S_{\text{sf}} \\ &= H_S - \omega S_{\text{sf}} + U^\dagger(t)H_{\text{DM}}(t)U(t), \end{aligned} \quad (\text{B6})$$

where $H(t) = H_S + H_{\text{DM}}(t)$ is given by Eq. (1). Since H_S preserves the number of spin flips we have $U^\dagger(t)H_S U(t) = H_S$. The DMI couple states whose number of spin flips differ by one. Defining P_n as the projection operator onto the subspace with n spin flips, the equation above can be written as

is characterized by the Chern of its energy bands [3]. Let us consider the Hamiltonian \hat{H} (in this appendix we follow Ref. [3] and use the hat notation \hat{O} to explicitly distinguish operators/operator vectors from vectors and matrices whose elements are complex numbers) which is diagonal in the momentum basis:

$$\hat{H} = \sum_{\mathbf{k}} \hat{\psi}_{\mathbf{k}}^\dagger \mathcal{H}_{\mathbf{k}} \hat{\psi}_{\mathbf{k}} = \sum_{\mathbf{k}} \hat{\psi}_{\mathbf{k}\alpha}^\dagger (\mathcal{H}_{\mathbf{k}})_{\alpha\beta} \hat{\psi}_{\mathbf{k}\beta}, \quad (\text{C1})$$

where $\hat{\psi}_{\mathbf{k}}^\dagger$ is a vector of creation operators with components $\hat{\psi}_{\mathbf{k}\alpha}^\dagger$ with $\alpha = 1, \dots, M$, where M is the number of internal degrees of freedom (e.g. number of atoms in the unit cell) and $\mathcal{H}_{\mathbf{k}}$ is the $(M \times M)$ matrix characterizing the Hamiltonian. In the equation above and for the rest of this appendix we use Einstein summation notation for Greek indices.

The eigenstates of \hat{H} may be obtained by computing the eigenstates of $\mathcal{H}_{\mathbf{k}}$. The eigenstate from the n^{th} band are obtained by solving the eigenvalue equation

$$\mathcal{H}_{\mathbf{k}} \phi_{n\mathbf{k}} = \varepsilon_n \phi_{n\mathbf{k}}. \quad (\text{C2})$$

Then, the Chern number \mathcal{C}_n for this band is obtained by integrating the z component of the Berry curvature over the Brillouin zone (BZ) [90, 91]

$$\mathcal{C}_n = \frac{1}{2\pi} \int_{\text{BZ}} d^2\mathbf{k} \mathcal{B}_{n\mathbf{k}}^z, \quad (\text{C3})$$

where

$$\mathcal{B}_{n\mathbf{k}}^k = -\epsilon_{ijk} \text{Im} [\partial_i \phi_{n\mathbf{k}\alpha}^* \partial_j \phi_{n\mathbf{k}\alpha}] \quad (\text{C4})$$

is the k^{th} component of the Berry curvature of the n^{th} band at momentum \mathbf{k} , $\phi_{n\mathbf{k}\alpha}$ is the α^{th} component of the vector $\phi_{n\mathbf{k}}$, $\partial_i = \partial/\partial k_i$ is the derivative with respect to the i^{th} component of the momentum, and ϵ_{ijk} is the Levi-Civita symbol in three dimensions (the indices i, j, k take the values x, y, z).

2. Effective TRS

The system described by the Hamiltonian $\hat{\mathcal{H}}$ [Eq. (C1)] has an effective time-reversal symmetry if there is a unitary matrix U acting on the internal degrees of freedom and an orthonormal 3×3 matrix O such that

$$U^\dagger \mathcal{H}_{\mathbf{k}'} U = \mathcal{H}_{\mathbf{k}}, \quad \mathbf{k}' = O\mathbf{k}, \quad (\text{C5})$$

is satisfied. If this symmetry is present, the system is topologically trivial in the sense that its Chern numbers vanish.

To show this, we note that when Eq. (C2) is satisfied then the equation

$$\mathcal{H}_{\mathbf{k}}^* \phi_{n\mathbf{k}}^* = \varepsilon_n \phi_{n\mathbf{k}}^*, \quad (\text{C6})$$

is also satisfied. By acting with U on the left and using Eq. (C5) we obtain

$$U \mathcal{H}_{\mathbf{k}}^* \phi_{n\mathbf{k}}^* = \mathcal{H}_{\mathbf{k}'} U \phi_{n\mathbf{k}}^* = \varepsilon_n U \phi_{n\mathbf{k}}^*, \quad (\text{C7})$$

where we used $UU^\dagger = 1$ as U is a unitary transformation. Therefore if $\phi_{n\mathbf{k}}$ is an eigenstate of $\mathcal{H}_{\mathbf{k}}$ then $U \phi_{n\mathbf{k}}^*$ is an eigenstate of $\mathcal{H}_{\mathbf{k}'}$ with the same energy ε_n given that the effective TRS symmetry (C5) is present.

Let us now compare the Berry curvature at \mathbf{k} and \mathbf{k}' for a given band n . Using Eq. (C4) and the fact that $U \phi_{n\mathbf{k}}$ is the n^{th} eigenstate of $h_{\mathbf{k}'}$ we have

$$\begin{aligned} \mathcal{B}_{n\mathbf{k}'}^z &= -\epsilon_{ijk} \text{Im} \left[\partial_i (U_{\alpha\beta} \phi_{n\mathbf{k}\beta}^*)^* \partial_j (U_{\alpha\beta} \phi_{n\mathbf{k}\beta}^*) \right] \\ &= -\epsilon_{ijk} \text{Im} \left[\partial_i (U_{\beta\alpha}^\dagger \phi_{n\mathbf{k}\beta}) \partial_j (U_{\alpha\beta} \phi_{n\mathbf{k}\beta}^*) \right] \\ &= -\epsilon_{ijk} \text{Im} \left[\partial_i \phi_{n\mathbf{k}\alpha} \partial_j \phi_{n\mathbf{k}\alpha}^* \right] \\ &= -\epsilon_{jik} \text{Im} \left[\partial_j \phi_{n\mathbf{k}\alpha} \partial_i \phi_{n\mathbf{k}\alpha}^* \right], \end{aligned} \quad (\text{C8})$$

where in the third line we used $U_{\beta\alpha}^\dagger U_{\alpha\beta} = \delta_{\alpha\beta}$. Comparing the equation above with Eq. (C4) and noting that $\epsilon_{jik} = -\epsilon_{ijk}$ we obtain

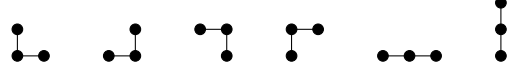
$$\mathcal{B}_{n\mathbf{k}'}^k = -\mathcal{B}_{n\mathbf{k}}^k. \quad (\text{C9})$$

Therefore, the contributions to the integral (C3) at momenta \mathbf{k} and \mathbf{k}' cancel each other and the Chern numbers vanish.

Appendix D: Three-magnon bound states

In this section we obtain the lowest energy of the three-magnon states in order to find the detuning Δ between the TMBSs and the three-magnon states when the DMI is driven. We use first-order perturbation theory where the unperturbed Hamiltonian H_0 and the perturbation V_1 are given by Eq. (B3a). In the limit $J_z \gg J_\perp$ the three-magnon spectrum splits into three branches: three-magnon bound states, one TMBSs and a single magnon and 3 single-magnon states. The three-magnon bound states have the lowest energy and are given by the Fourier

transform of three adjacent spin flips. There are six states with three neighboring spin flips with unperturbed energy $3B + 4J_z$, these are



where each black dot represents a spin flip. The first four states are coupled to first order in V_1 since only the hopping of one spin flip (represented by the black dot) is required to go from one state to another. In the subspace of these four state, which in momentum space are

$$\left(|\mathbf{k}, \hat{x}, \hat{y}\rangle \quad |\mathbf{k}, \hat{x}, \hat{x} + \hat{y}\rangle \quad |\mathbf{k}, -\hat{x}, -\hat{y}\rangle \quad |\mathbf{k}, \hat{y}, \hat{x} + \hat{y}\rangle \right), \quad (\text{D1})$$

the perturbation V_1 is given by

$$V_1 = \frac{J_\perp}{2} \begin{pmatrix} 0 & e^{ik_x/3} & 0 & e^{ik_y/3} \\ e^{-ik_x/3} & 0 & e^{ik_y/3} & 0 \\ 0 & e^{-ik_y/3} & 0 & e^{-ik_x/3} \\ e^{-ik_y/3} & 0 & e^{ik_x/3} & 0 \end{pmatrix}, \quad (\text{D2})$$

which has eigenvalues $3B + 4J_z$ (doubly degenerate), $3B + 4J_z + J_\perp$ and $3B + 4J_z - J_\perp$. Hence, the lowest-energy three-magnon state is (to first order in V_1) $3B + 4J_z - J_\perp$.

Appendix E: Hamiltonian in the ribbon geometry

To write the Hamiltonian for the ribbon geometry we define the vector $\psi_{\mathbf{k}} = (|\mathbf{k}\rangle \quad |\mathbf{k}, e_x\rangle \quad |\mathbf{k}, e_y\rangle)^T$. Then, the effective Hamiltonian with periodic boundary conditions can be written as

$$\tilde{H} = \sum_{\mathbf{k}} \psi_{\mathbf{k}}^\dagger \tilde{H}_{\mathbf{k}} \psi_{\mathbf{k}}, \quad (\text{E1})$$

where $\tilde{H}_{\mathbf{k}}$ is given by Eq. (24). By using the partial Fourier transform

$$\psi_{k_y y} = \frac{1}{L} \sum_{k_y} e^{ik_y y} U_{k_y} \psi_{\mathbf{k}}, \quad (\text{E2})$$

where $U_{k_y} = \text{diag}(1, 1, e^{-ik_y/2})$. in Eq. (E1) we obtain the Hamiltonian with open boundary conditions:

$$H_{\text{op}} = \sum_{k_x} \sum_{y=1}^{L-1} \left[\psi_{k_x y}^\dagger \boldsymbol{\mu} \psi_{k_x y} + \left(\psi_{k_x y+1}^\dagger \mathbf{T} \psi_{k_x y} + \text{h.c.} \right) \right], \quad (\text{E3})$$

where the matrices $\boldsymbol{\mu}$ and \mathbf{T} are given by

$$\boldsymbol{\mu} = \begin{pmatrix} \mu_{11} & -ids_x & -id/2 \\ ids_x & \mu_{22} & \frac{d^2 s_x}{2\delta} - \frac{J_\perp^2 c_x}{J_z} \\ id/2 & \frac{d^2 s_x}{2\delta} - \frac{J_\perp^2 c_x}{J_z} & \mu_{33} \end{pmatrix}, \quad (\text{E4})$$

where

$$\mu_{11} = B + 2J_z - \omega - J_{\perp} \cos k_x, \quad (\text{E5})$$

$$\mu_{22} = 2B + 3J_z - 2\omega - \frac{J_{\perp}^2(1 + c_x^2)}{J_z} + \frac{d^2(2 - c_x^2)}{\delta}, \quad (\text{E6})$$

$$\mu_{33} = 2B + 3J_z - 2\omega - \frac{J_{\perp}^2(1 + c_x^2)}{J_z} + \frac{d^2}{2\delta}, \quad (\text{E7})$$

where $\delta = B + J_z - \omega$ and

$$\mathbf{T} = - \begin{pmatrix} J_{\perp}/2 & 0 & -Id^2/2 \\ 0 & J_{\perp}^2/2J_z & J_{\perp}^2 c_x/J_z + d^2 s_x/2\delta \\ 0 & 0 & (J_{\perp}^2/J_z + d^2/\delta)/4 \end{pmatrix}. \quad (\text{E8})$$

-
- [1] M. Z. Hasan and C. L. Kane, Colloquium: Topological insulators, *Rev. Mod. Phys.* **82**, 3045 (2010).
- [2] X.-L. Qi and S.-C. Zhang, Topological insulators and superconductors, *Rev. Mod. Phys.* **83**, 1057 (2011).
- [3] C.-K. Chiu, J. C. Y. Teo, A. P. Schnyder, and S. Ryu, Classification of topological quantum matter with symmetries, *Rev. Mod. Phys.* **88**, 035005 (2016).
- [4] L. Lu, J. D. Joannopoulos, and M. Soljačić, Topological photonics, *Nature Photonics* **8**, 821 (2014).
- [5] T. Ozawa, H. M. Price, A. Amo, N. Goldman, M. Hafezi, L. Lu, M. C. Rechtsman, D. Schuster, J. Simon, O. Zilberberg, and I. Carusotto, Topological photonics, *Rev. Mod. Phys.* **91**, 015006 (2019).
- [6] N. Goldman, J. Budich, and P. Zoller, Topological quantum matter with ultracold gases in optical lattices, *Nature Phys* **12**, 639 (2016).
- [7] N. R. Cooper, J. Dalibard, and I. B. Spielman, Topological bands for ultracold atoms, *Rev. Mod. Phys.* **91**, 015005 (2019).
- [8] R. Shindou, R. Matsumoto, S. Murakami, and J. Ohe, Topological chiral magnonic edge mode in a magnonic crystal, *Phys. Rev. B* **87**, 174427 (2013).
- [9] L. Zhang, J. Ren, J.-S. Wang, and B. Li, Topological magnon insulator in insulating ferromagnet, *Phys. Rev. B* **87**, 144101 (2013).
- [10] M. Malki and G. S. Uhrig, Topological magnetic excitations, *Europhysics Letters* **132**, 20003 (2020).
- [11] X. S. Wang and X. R. Wang, Topological magnonics, *Journal of Applied Physics* **129**, 151101 (2021).
- [12] P. A. McClarty, Topological magnons: A review, *Annual Review of Condensed Matter Physics* **13**, 171 (2022).
- [13] F. Zhuo, J. Kang, A. Manchon, and Z. Cheng, Topological phases in magnonics, *Advanced Physics Research* **4**, 2300054 (2025).
- [14] H. Katsura, N. Nagaosa, and P. A. Lee, Theory of the thermal Hall effect in quantum magnets, *Phys. Rev. Lett.* **104**, 066403 (2010).
- [15] R. Matsumoto and S. Murakami, Theoretical prediction of a rotating magnon wave packet in ferromagnets, *Phys. Rev. Lett.* **106**, 197202 (2011).
- [16] R. Matsumoto and S. Murakami, Rotational motion of magnons and the thermal Hall effect, *Phys. Rev. B* **84**, 184406 (2011).
- [17] Y. Onose, T. Ideue, H. Katsura, Y. Shiomi, N. Nagaosa, and Y. Tokura, Observation of the magnon Hall effect, *Science* **329**, 297 (2010).
- [18] T. Ideue, Y. Onose, H. Katsura, Y. Shiomi, S. Ishiwata, N. Nagaosa, and Y. Tokura, Effect of lattice geometry on magnon Hall effect in ferromagnetic insulators, *Phys. Rev. B* **85**, 134411 (2012).
- [19] K. v. Klitzing, G. Dorda, and M. Pepper, New method for high-accuracy determination of the fine-structure constant based on quantized Hall resistance, *Phys. Rev. Lett.* **45**, 494 (1980).
- [20] D. J. Thouless, M. Kohmoto, M. P. Nightingale, and M. den Nijs, Quantized Hall conductance in a two-dimensional periodic potential, *Phys. Rev. Lett.* **49**, 405 (1982).
- [21] F. D. M. Haldane, Model for a quantum Hall effect without Landau levels: Condensed-matter realization of the "parity anomaly", *Phys. Rev. Lett.* **61**, 2015 (1988).
- [22] T. Holstein and H. Primakoff, Field dependence of the intrinsic domain magnetization of a ferromagnet, *Phys. Rev.* **58**, 1098 (1940).
- [23] A. Mook, J. Henk, and I. Mertig, Edge states in topological magnon insulators, *Phys. Rev. B* **90**, 024412 (2014).
- [24] X. S. Wang, Y. Su, and X. R. Wang, Topologically protected unidirectional edge spin waves and beam splitter, *Phys. Rev. B* **95**, 014435 (2017).
- [25] X. S. Wang, H. W. Zhang, and X. R. Wang, Topological magnonics: A paradigm for spin-wave manipulation and device design, *Phys. Rev. Appl.* **9**, 024029 (2018).
- [26] B. Hetényi, A. Mook, J. Klinovaja, and D. Loss, Long-distance coupling of spin qubits via topological magnons, *Phys. Rev. B* **106**, 235409 (2022).
- [27] A. Mook, K. Plekhanov, J. Klinovaja, and D. Loss, Interaction-stabilized topological magnon insulator in ferromagnets, *Phys. Rev. X* **11**, 021061 (2021).
- [28] J. Habel, A. Mook, J. Willsher, and J. Knolle, Breakdown of chiral edge modes in topological magnon insulators, *Phys. Rev. B* **109**, 024441 (2024).
- [29] J. Hanus, Bound states in the Heisenberg ferromagnet, *Phys. Rev. Lett.* **11**, 336 (1963).
- [30] M. Wortis, Bound states of two spin waves in the Heisenberg ferromagnet, *Phys. Rev.* **132**, 85 (1963).
- [31] A. Mook, R. Hoyer, J. Klinovaja, and D. Loss, Magnons, magnon bound pairs, and their hybrid spin-multipolar topology, *Phys. Rev. B* **107**, 064429 (2023).
- [32] J. B. Torrance and M. Tinkham, Excitation of multiple-magnon bound states in $\text{CoCl}_2 \cdot 2\text{H}_2\text{O}$, *Phys. Rev.* **187**, 595 (1969).
- [33] D. Petitgrand, A. Brun, and P. Meyer, Magnetic field dependence of spin waves and two magnon bound states in FeI_2 , *Journal of Magnetism and Magnetic Materials* **15-18**, 381 (1980).

- [34] A. Fert, D. Bertrand, J. Leotin, J. Ousset, J. Magariño, and J. Tuchendler, Excitation of two spin deviations by far infrared absorption in FeI_2 , *Solid State Communications* **26**, 693 (1978).
- [35] T. Fukuhara, P. Schauß, M. Endres, S. Hild, M. Cheneau, I. Bloch, and C. Gross, Microscopic observation of magnon bound states and their dynamics, *Nature* **502**, 76 (2013).
- [36] X. Qin, F. Mei, Y. Ke, L. Zhang, and C. Lee, Topological magnon bound states in periodically modulated Heisenberg XXZ chains, *Phys. Rev. B* **96**, 195134 (2017).
- [37] X. Qin, F. Mei, Y. Ke, L. Zhang, and C. Lee, Topological magnon bound states in periodically modulated Heisenberg XXZ chains, *Phys. Rev. B* **96**, 195134 (2017).
- [38] Y. Endoh, Y. Ajiro, H. Shiba, and H. Yoshizawa, Resonant coupling between one- and two-magnon excitations in tetramethylamine manganese trichloride (TMMC), *Phys. Rev. B* **30**, 4074(R) (1984).
- [39] I. U. Heilmann, J. K. Kjems, Y. Endoh, G. F. Reiter, G. Shirane, and R. J. Birgeneau, One- and two-magnon excitations in a one-dimensional antiferromagnet in a magnetic field, *Phys. Rev. B* **24**, 3939 (1981).
- [40] X. Bai, S.-S. Zhang, Z. Dun, H. Zhang, Q. Huang, H. Zhou, M. B. Stone, A. I. Kolesnikov, F. Ye, C. D. Batista, *et al.*, Hybridized quadrupolar excitations in the spin-anisotropic frustrated magnet FeI_2 , *Nat. Phys.* **17**, 467 (2021).
- [41] X. Bai, S.-S. Zhang, H. Zhang, Z. Dun, W. A. Phelan, V. O. Garlea, M. Mourigal, and C. D. Batista, Instabilities of heavy magnons in an anisotropic magnet, *Nat Commun* **14**, 4199 (2023).
- [42] I. Dzyaloshinsky, A thermodynamic theory of “weak” ferromagnetism of antiferromagnetics, *Journal of Physics and Chemistry of Solids* **4**, 241 (1958).
- [43] T. Moriya, Anisotropic superexchange interaction and weak ferromagnetism, *Phys. Rev.* **120**, 91 (1960).
- [44] T. Oka and H. Aoki, Photovoltaic Hall effect in graphene, *Phys. Rev. B* **79**, 081406 (2009).
- [45] N. H. Lindner, G. Refael, and V. Galitski, Floquet topological insulator in semiconductor quantum wells, *Nature Phys* **7**, 490 (2011).
- [46] T. Kitagawa, E. Berg, M. Rudner, and E. Demler, Topological characterization of periodically driven quantum systems, *Phys. Rev. B* **82**, 235114 (2010).
- [47] M. S. Rudner and N. H. Lindner, Band structure engineering and non-equilibrium dynamics in Floquet topological insulators, *Nat Rev Phys* **2**, 229 (2020).
- [48] M. S. Rudner and N. H. Lindner, The Floquet engineer’s handbook (2020), arXiv:2003.08252 [cond-mat.mes-hall].
- [49] T. Oka and S. Kitamura, Floquet engineering of quantum materials, *Annual Review of Condensed Matter Physics* **10**, 387 (2019).
- [50] S. A. Owerre, Floquet topological magnons, *Journal of Physics Communications* **1**, 021002 (2017).
- [51] S. Owerre, Photoinduced topological phase transitions in topological magnon insulators, *Sci Rep* **8**, 4431 (2018).
- [52] Z. Zhang, W. Feng, Y. Yao, and B. Tang, Photoinduced Floquet topological magnons in a ferromagnetic checkerboard lattice, *Physics Letters A* **414**, 127630 (2021).
- [53] Q.-H. Chen, F.-J. Huang, Y.-P. Fu, and H. Su, Floquet no-go theorem and engineering topological magnons, *Phys. Rev. B* **111**, 064426 (2025).
- [54] F. Kammerbauer, F. Freimuth, R. Frömter, Y. Mokrousov, and M. Kläui, Dzyaloshinskii–Moriya interaction and its current-induced manipulation, *Journal of the Physical Society of Japan* **92**, 081007 (2023).
- [55] Y. Meng, F. Meng, M. Hou, Q. Zheng, B. Wang, R. Zhu, C. Feng, and G. Yu, Regulation of interfacial Dzyaloshinskii–Moriya interaction in ferromagnetic multilayers, *Journal of Physics: Condensed Matter* **36**, 193001 (2024).
- [56] N. S. Gusev, A. V. Sadovnikov, S. A. Nikitov, M. V. Sapozhnikov, and O. G. Udalov, Manipulation of the Dzyaloshinskii–Moriya interaction in Co/Pt multilayers with strain, *Phys. Rev. Lett.* **124**, 157202 (2020).
- [57] Q. Cui, J. Liang, Z. Shao, P. Cui, and H. Yang, Strain-tunable ferromagnetism and chiral spin textures in two-dimensional Janus chromium dichalcogenides, *Phys. Rev. B* **102**, 094425 (2020).
- [58] C. Deger, Strain-enhanced Dzyaloshinskii–Moriya interaction at Co/Pt interfaces, *Sci Rep* **10**, 12314 (2020).
- [59] H. Yang, O. Boule, V. Cros, A. Fert, and M. Chshiev, Controlling Dzyaloshinskii–Moriya interaction via chirality dependent atomic-layer stacking, insulator capping and electric field, *Sci Rep* **8**, 12356 (2018).
- [60] W. Zhang, H. Zhong, R. Zang, Y. Zhang, S. Yu, G. Han, G. L. Liu, S. S. Yan, S. Kang, and L. M. Mei, Electrical field enhanced interfacial Dzyaloshinskii–Moriya interaction in MgO/Fe/Pt system, *Applied Physics Letters* **113**, 122406 (2018).
- [61] Y. G. Semenov, X. Xu, J. A. Boulton, and K. W. Kim, Electrical control of Dzyaloshinskii–Moriya interactions in magnetic Weyl semimetals, *Phys. Rev. B* **108**, 134428 (2023).
- [62] J. Liu, M. Shi, J. Lu, and M. P. Anantram, Analysis of electrical-field-dependent Dzyaloshinskii–Moriya interaction and magnetocrystalline anisotropy in a two-dimensional ferromagnetic monolayer, *Phys. Rev. B* **97**, 054416 (2018).
- [63] J. Chen, C. Gui, and S. Dong, Dzyaloshinskii–Moriya interaction torques and domain wall dynamics in van der Waals heterostructures, *Phys. Rev. B* **110**, L060406 (2024).
- [64] T. Fukui, Y. Hatsugai, and H. Suzuki, Chern numbers in discretized Brillouin zone: efficient method of computing (spin) Hall conductances, *Journal of the Physical Society of Japan* **74**, 1674 (2005).
- [65] M. S. Rudner, N. H. Lindner, E. Berg, and M. Levin, Anomalous edge states and the bulk-edge correspondence for periodically driven two-dimensional systems, *Phys. Rev. X* **3**, 031005 (2013).
- [66] K. S. Burch, D. Mandrus, and J. Park, Magnetism in two-dimensional van der Waals materials, *Nature* **563**, 47 (2018).
- [67] J.-G. Park, Opportunities and challenges of 2d magnetic van der Waals materials: magnetic graphene?, *Journal of Physics: Condensed Matter* **28**, 301001 (2016).
- [68] S. Mañas-Valero, T. van der Sar, R. A. Duine, and B. van Wees, Fundamentals and applications of van der Waals magnets in magnon spintronics, *Newton* **1**, 10.1016/j.newton.2025.100018 (2025).
- [69] C. Gong, L. Li, Z. Li, H. Ji, A. Stern, Y. Xia, T. Cao, W. Bao, C. Wang, Y. Wang, *et al.*, Discovery of intrinsic ferromagnetism in two-dimensional van der Waals crystals, *Nature* **546**, 265 (2017).
- [70] J. L. Lado and J. Fernández-Rossier, On the origin of magnetic anisotropy in two dimensional CrI_3 , *2D Materials* **4**, 035002 (2017).

- [71] B. Huang, G. Clark, E. Navarro-Moratalla, D. R. Klein, R. Cheng, K. L. Seyler, D. Zhong, E. Schmidgall, M. A. McGuire, D. H. Cobden, *et al.*, Layer-dependent ferromagnetism in a van der Waals crystal down to the monolayer limit, *Nature* **546**, 270 (2017).
- [72] A.-Y. Lu, H. Zhu, J. Xiao, C.-P. Chuu, Y. Han, M.-H. Chiu, C.-C. Cheng, C.-W. Yang, K.-H. Wei, Y. Yang, *et al.*, Janus monolayers of transition metal dichalcogenides, *Nature Nanotech* **12**, 744 (2017).
- [73] J. Zhang, S. Jia, I. Kholmanov, L. Dong, D. Er, W. Chen, H. Guo, Z. Jin, V. B. Shenoy, L. Shi, *et al.*, Janus monolayer transition-metal dichalcogenides, *ACS Nano* **11**, 8192 (2017).
- [74] J. Liang, W. Wang, H. Du, A. Hallal, K. Garcia, M. Chshiev, A. Fert, and H. Yang, Very large Dzyaloshinskii–Moriya interaction in two-dimensional Janus manganese dichalcogenides and its application to realize skyrmion states, *Phys. Rev. B* **101**, 184401 (2020).
- [75] J. Yuan, Y. Yang, Y. Cai, Y. Wu, Y. Chen, X. Yan, and L. Shen, Intrinsic skyrmions in monolayer Janus magnets, *Phys. Rev. B* **101**, 094420 (2020).
- [76] C. Xu, J. Feng, S. Prokhorenko, Y. Nahas, H. Xiang, and L. Bellaïche, Topological spin texture in Janus monolayers of the chromium trihalides $\text{Cr}(\text{I}, \text{X})_3$, *Phys. Rev. B* **101**, 060404 (2020).
- [77] T. Miyamoto, H. Yada, H. Yamakawa, and H. Okamoto, Ultrafast modulation of polarization amplitude by terahertz fields in electronic-type organic ferroelectrics, *Nat Commun* **4**, 2586 (2013).
- [78] R. Mankowsky, A. von Hoegen, M. Först, and A. Cavalleri, Ultrafast reversal of the ferroelectric polarization, *Phys. Rev. Lett.* **118**, 197601 (2017).
- [79] Y. Wang, M. S. Hossain, T. Li, Y. Xiong, C. Le, J. Kuebler, N. Raghavan, L. Fernandez-Ballester, X. Hong, A. Sinitskii, *et al.*, Ultrafast dynamics of ferroelectric polarization of NbOI_2 captured with femtosecond electron diffraction, *Nat Commun* **16**, 8132 (2025).
- [80] D. Luo, B. Zhang, E. J. Sie, C. M. Nyby, Q. Fan, X. Shen, A. H. Reid, M. C. Hoffmann, S. Weathersby, J. Wen, *et al.*, Ultrafast optomechanical strain in layered GeS , *Nano Letters* **23**, 2287 (2023).
- [81] J. Gollwitzer, J. Z. Kaaret, Y. E. Suyolcu, G. Khalsa, R. C. Fernandes, O. Gorobtsov, S. Buchenau, C. You, J. Higgins, R. S. Russell, Z. Shao, Y. A. Birkhölzer, T. Sato, M. Chollet, G. Coslovich, M. Brützmam, C. Gungushev, J. W. Harter, A. S. Disa, D. G. Schlom, N. A. Benedek, and A. Singer, Picosecond expansion in LaAlO_3 resonantly driven by infrared-active phonons, *Phys. Rev. Lett.* **135**, 116906 (2025).
- [82] A. Browaeys and T. Lahaye, Many-body physics with individually controlled Rydberg atoms, *Nat. Phys.* **16**, 132 (2020).
- [83] H. Kuji, M. Kunimi, and T. Nikuni, Proposal for realizing quantum-spin systems on a two-dimensional square lattice with Dzyaloshinskii–Moriya interaction by Floquet engineering using Rydberg atoms, *Phys. Rev. A* **112**, 022614 (2025).
- [84] L.-M. Duan, E. Demler, and M. D. Lukin, Controlling spin exchange interactions of ultracold atoms in optical lattices, *Phys. Rev. Lett.* **91**, 090402 (2003).
- [85] S. Trotzky, P. Cheinet, S. Fölling, M. Feld, U. Schnorrberger, A. M. Rey, A. Polkovnikov, E. A. Demler, M. D. Lukin, and I. Bloch, Time-resolved observation and control of superexchange interactions with ultracold atoms in optical lattices, *Science* **319**, 295 (2008).
- [86] M. Gong, Y. Qian, M. Yan, V. W. Scarola, and C. Zhang, Dzyaloshinskii–Moriya interaction and spiral order in spin-orbit coupled optical lattices, *Sci Rep* **5**, 10050 (2015).
- [87] J. Radić, A. Di Ciolo, K. Sun, and V. Galitski, Exotic quantum spin models in spin-orbit-coupled Mott insulators, *Phys. Rev. Lett.* **109**, 085303 (2012).
- [88] W. S. Cole, S. Zhang, A. Paramekanti, and N. Trivedi, Bose-Hubbard models with synthetic spin-orbit coupling: Mott insulators, spin textures, and superfluidity, *Phys. Rev. Lett.* **109**, 085302 (2012).
- [89] C. Cohen-Tannoudji, J. Dupont-Roc, and G. Grynberg, *Atom-photon interactions: basic processes and applications* (John Wiley & Sons, 1998).
- [90] J. K. Asbóth, L. Oroszlány, and A. Pályi, *A Short Course on Topological Insulators*, Vol. 919 (Springer, 2016) p. 166.
- [91] D. Xiao, M.-C. Chang, and Q. Niu, Berry phase effects on electronic properties, *Rev. Mod. Phys.* **82**, 1959 (2010).